Proton capture cross sections of the ruthenium isotopes

J. Bork, H. Schatz, and F. Käppeler
Forschungszentrum Karlsruhe, Institut für Kernphysik, Postfach 3640, D-76021 Karlsruhe, Germany

T. Rauscher
Institut für Physik, Universität Basel, Klingelbergstrasse 82, CH-4056 Basel, Switzerland
(Received 12 March 1998)

The proton capture cross sections of the stable ruthenium isotopes 96, 98, 99, and 104 have been measured by means of the activation method in the proton energy range between 1.5 and 3 MeV. Thin layers of natural ruthenium were irradiated at the Karlsruhe 3.75 MV Van de Graaff accelerator with proton beams of 20–50 μA. The activity induced by (p,γ) reactions was measured with a calibrated HPGe detector. In this way, six (p,γ) cross sections for populating ground states and isomers in four different Rh isotopes could be determined simultaneously with systematic uncertainties of typically 4–5 %. The fact that experimental data are almost completely missing in the $A>70$ region illustrates the need of checking and complementing the statistical model calculations which are so far the only data used in *p* process studies.
[S0556-2813(98)05307-2]

PACS number(s): 25.40.Lw, 26.30.+k, 27.60.+j, 97.10.Tk

I. INTRODUCTION

The elements heavier than iron are predominantly produced via neutron capture and β^- decays in the *s* and *r* processes, as first suggested by Burbidge, Burbidge, Fowler, and Hoyle (BBFH) [1]. However, there are 32 stable isotopes between ^{74}Se and ^{196}Hg on the proton-rich side of the valley of stability that are shielded from the neutron capture processes by stable isobars. These so-called *p* nuclei are typically 10–100 times less abundant than their neutron-rich isotopes, but their abundance curve almost parallels those of the *r* and *s* nuclei. This leads to the conclusion that the *p* nuclei originate from an *r*- and *s*-process seed that is modified by either photodisintegration or proton capture.

The presently favored sites for photodisintegration reactions are the explosively burning O/Ne layers in supernovae of type II (SN II), where temperatures of $2-3\times10^9$ K are reached [2]. While the abundances of most heavy *p* nuclei are reproduced within a factor of 3, this model implies a significant underproduction of the abundant *p* nuclei ^{92}Mo, ^{94}Mo, ^{96}Ru, and ^{98}Ru (Fig. 1). This problem results from the lack of sufficient seed nuclei to account for their rather large isotopic abundances of 14.84%, 9.25%, 5.52%, and 1.88%, respectively.

An alternative origin of these nuclei could be via (p,γ) reactions. High temperatures and proton densities are required for these reactions to proceed with significant rates. While BBFH suggested the exploding H-rich outer layer of SN II as a possible site, this was later proved impossible [3]. Astrophysically more plausible are events where hydrogen is burnt explosively under degenerate conditions as it occurs in novae or x-ray bursters [4]. Another possible site are SNe Ia, where free protons are released via the ^{12}C(^{12}C,p)^{23}Na channel during explosive carbon burning in the core. Theoretically suggested, but yet unobserved candidates are Thorne-Żytkow objects, which develop from a close binary system, when the neutron star sinks into the center of the red giant. A fully convective envelope transports seed nuclei to the burning zone right above the neutron core [5] where temperatures of $1-2\times10^9$ K and densities of 10^3-10^4 g/cm^3 are reached. The produced *p* nuclei are then flushed back to the outer layers of the red giant. Their observation in the envelope would be a proof for the existence of such an object. However, recent calculations indicate that Thorne-Żytkow objects are gravitationally unstable which puts their existence into question [6,7].

Extended network calculations have been performed simulating nucleosynthesis in the discussed sites, but all studies had to rely on theoretical (p,γ) rates based on the Hauser-Feshbach model, since experimental data are almost completely missing in the mass region $A\geqslant70$. Therefore, systematic (p,γ) cross section measurements were initiated at the Karlsruhe Van de Graaff accelerator in the $A\sim100$ region using the activation technique. The experimental setup and the problems related to the irradiations and data analysis were recently reported together with the (p,γ) cross

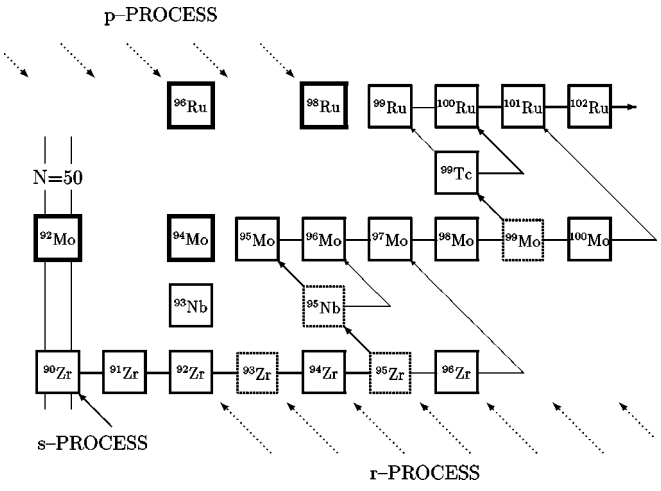

FIG. 1. The main nucleosynthesis mechanisms in the mass region between Zr and Ru are the *s* and *r* processes. Both reaction flows bypass the abundant *p* nuclei ^{92}Mo, ^{94}Mo, ^{96}Ru, and ^{98}Ru.

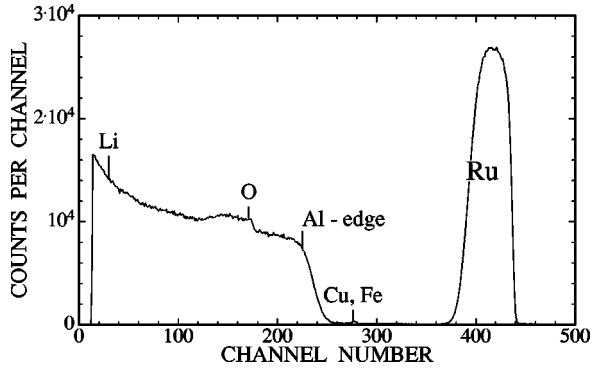

FIG. 2. RBS spectrum of an activation sample. The ruthenium layer exhibits a certain oxygen content which shows up on top of the contribution from the aluminum backing. Traces of iron and/or copper are also visible in the spectrum.

sections for a number of molybdenum isotopes [8]. This work is being complemented by the present study of various ruthenium nuclei.

II. TARGET PREPARATION

The activation technique does not require one to use enriched targets, because each isotope is represented in the γ spectrum by its characteristic lines, and even small quantities are sufficient for detection. Hence, the cross sections of several isotopes could be determined simultaneously by activating natural ruthenium.

Two points, however, have to be taken into account when preparing the samples: The target thickness should not exceed 3000 Å to keep the energy loss in the target within $\sim$30 keV, and the cohesion of the material on the backing has to be good enough to stand a proton bombardment of several hours. Both requirements are easily met when the samples are produced by sputtering thin Ru layers onto 1 mm thick aluminum disks. Aluminum was chosen for several reasons: the good heat conductivity allows for effective cooling during the proton irradiations, the low atomic number yields sufficiently good separation of the Rutherford backscattering (RBS) signal from that of the Ru layers (see below), and proton captures are producing stable ^{28}Si, thus avoiding background activities.

The target thickness was determined in two ways, by RBS and via x-ray fluorescence (XRF) analysis. Figure 2 shows a typical RBS spectrum of ruthenium sputtered onto a thick aluminum backing. The width of the Ru peak is due to the difference in energy of the projectiles scattered in the front and back of the ruthenium layer and can be used to determine the thickness of the layer [9]:

$$\Delta E = x[S], \tag{1}$$

with the energy loss factor $[S]$ and the target thickness x. Alternatively, the area density follows from the number of counts in the ruthenium peak and the height of the aluminum edge:

$$N_{\mathrm{Ru}} = \frac{A_{\mathrm{Ru}}\sigma_{\mathrm{Al}}\xi}{H_{\mathrm{Al}}\sigma_{\mathrm{Ru}}[\epsilon]_{\mathrm{Al}}}, \tag{2}$$

where N_{Ru} denotes the number of Ru atoms/cm^2, A_{Ru} the number of counts within the Ru peak, and H_{Al} the height of Al edge. The other parameters in this expression are the Rutherford cross sections σ, the width of the energy bin per channel, ξ, and the effective stopping cross section $[\epsilon]_{\mathrm{Al}}$ [10].

The oxygen feature in the RBS spectrum is relatively broad but is not shifted to lower energies. This shows that it is mostly related to the ruthenium layer. The Al backings contain traces of copper and lead, and seem to be particularly contaminated with lithium. This latter impurity is difficult to quantify in the RBS spectrum but is evident via the ^{8}Be activity induced in the proton irradiations.

The XRF analysis was carried out with a Siemens SRS 3000 crystal spectrometer that was operated with a rhodium anode. The induced characteristic x rays were analyzed with a LiF(100) crystal. The efficiency of the spectrometer was calibrated by the radiation emitted from five well-defined ruthenium samples which were prepared from a standard solution. With the RBS as well as with the XRF technique, the sample thickness could be determined with an accuracy of 3–4 %.

III. EXPERIMENTAL PROCEDURE

The cross sections were measured via the activation technique at the Karlsruhe 3.75 MV Van de Graaff accelerator. The investigated energy range between 1500 and 3500 keV was covered in 30 steps, each of the respective proton irradiations lasting several hours. The relevant parameters of these activations are summarized in Table I. The uncertainties in energy due to the width of the proton beam ($\Delta E/E = \pm 0.05\%$) and the 5 keV uncertainty of the energy calibration were always small compared to the energy loss in the target.

The beam current of 20 to 50 μA was measured with a digital current integrator and recorded in multichannel scaling (MCS) mode for the proper correction of the decay during the irradiations. The activation chamber was constructed as a Faraday cup with secondary electron suppression to ensure complete charge collection (Fig. 3) [8]. During the actual activations the RBS detector was operated with a reduced aperture of 0.2 mm diameter for monitoring the target performance.

After the irradiations, the induced γ activity was measured with a 265 cm^3 HPGe detector. At high proton energies, sufficient statistics were achieved for all investigated γ lines within the 10 h counting periods. At low energies, the smaller activity resulted in statistical uncertainties of up to $\sim$15% for the long-lived isotopes.

IV. DATA ANALYSIS AND RESULTS

The cross sections were deduced from the number of counts in the γ spectra measured after the activations. A typical example of such a spectrum is shown in Fig. 4. The most prominent lines in this spectrum originate from the decay of the ^{100}Rh ground state and represent the total (p,γ) cross section of ^{99}Ru. This clear signature is favored by relatively large γ intensities per decay, I_γ, and a half-life similar to the activation and counting times. In addition to the lines

TABLE I. Activations and sample characteristics.

Activations					Samples		
Run	Proton energy (keV)	Average beam current (μA)	Time (min)	Integrated charge (mC)	Sample number	Proton energy loss[a] (keV)	Number Density[b] (10^{17} atoms/cm^2)
1	1492	35	910	1902	54	28	18.6±0.6
2	1552	35	525	1096	53	27	18.6±0.6
3	1626	37	512	1136	29	12	8.4±0.2
4	1677	31	868	1509	52	27	19.1±0.6
5	1740	26	953	1494	28	16	11.4±0.3
6	1794	35	470	973	51	30	22.1±0.7
7	1884	31	990	1821	25	14	10.8±0.3
8	1972	35	922	1915	50	24	19.3±0.6
9	2062	39	536	1246	49	24	19.3±0.6
10	2112	43	868	2227	48	23	18.8±0.6
11	2172	45	341	1363	47	23	19.1±0.6
12	2217	48	765	2193	46	24	20.2±0.6
13	2272	52	330	1033	45	22	19.0±0.6
14	2388	44	841	2227	55	21	18.9±0.6
15	2430	42	951	2381	44	20	18.1±0.5
16	2527	52	471	1455	43	15	13.5±0.4
17	2576	47	246	659	60	22	20.8±0.6
18	2685	33	938	1858	42	14	13.1±0.4
19	2717	51	324	982	58	21	19.9±0.6
20	2822	39	568	1316	41	13	12.5±0.4
21	2897	51	894	2789	57	18	18.3±0.5
22	2982	39	905	2142	40	11	11.1±0.3
23	3017	45	328	887	56	23	23.4±0.7
24	3133	35	450	938	39	10	10.6±0.3
25	3212	42	909	2272	38	9	9.3±0.3
26	3252	35	170	351	36	11	11.2±0.3
27	3287	22	747	962	34	11	12.2±0.4
28	3412	23	180	250	35	10	10.9±0.3

[a]See text.
[b]Average of XRF and RBS results.

from the various induced Rh activities, strong background lines occur due to positron annihilation, the ^{97}Ru activity associated with the ^{97}Rh decay, and the ^{7}Be activity resulting from the above-mentioned lithium impurity in the aluminum backings.

The total number of decays can be deduced from the number of counts in a particular line, A, from the respective γ intensity I_γ, the detector efficiency ϵ_γ, and—if necessary—the cascade-summing corrections, C_k:

$$N=\frac{AC_k}{\epsilon_\gamma I_\gamma}. \tag{3}$$

The cross section is then calculated from the system of differential equations that describes the development of the number of nuclei in the isomer, $M(t)$, and in the ground state, $G(t)$, of a particular Rh isotope during the activation and during the activity counting with the Ge detector.

The corresponding expressions during activation are

$$\frac{dM}{dt}=\sigma_m\phi N_t-\lambda_m M(t) \tag{4}$$

and

$$\frac{dG}{dt}=\sigma_g\phi N_t-\lambda_g G(t)+\eta\sigma_m M(t). \tag{5}$$

These expressions hold also during the counting period, except that the proton capture terms vanish. The various quantities are the (p,γ) cross sections σ, the proton current ϕ, the decay rates λ, and the probability for an internal transition, η.

For constant proton current, these equations can be solved analytically. Instead, the cross sections were calculated by numerical integration using the recorded MCS spectrum to account for the instabilities of the proton beam current during the activation.

The analyzed reactions and the relevant properties of the product nuclei are summarized in Table II. With the activation technique it is in principle possible to separate the partial cross sections for populating the isomer and the ground state of the product nucleus. However, the isomers in ^{100}Rh and ^{105}Rh were too short lived and could not be detected in the present experiment. Accordingly, only the total (p,γ)

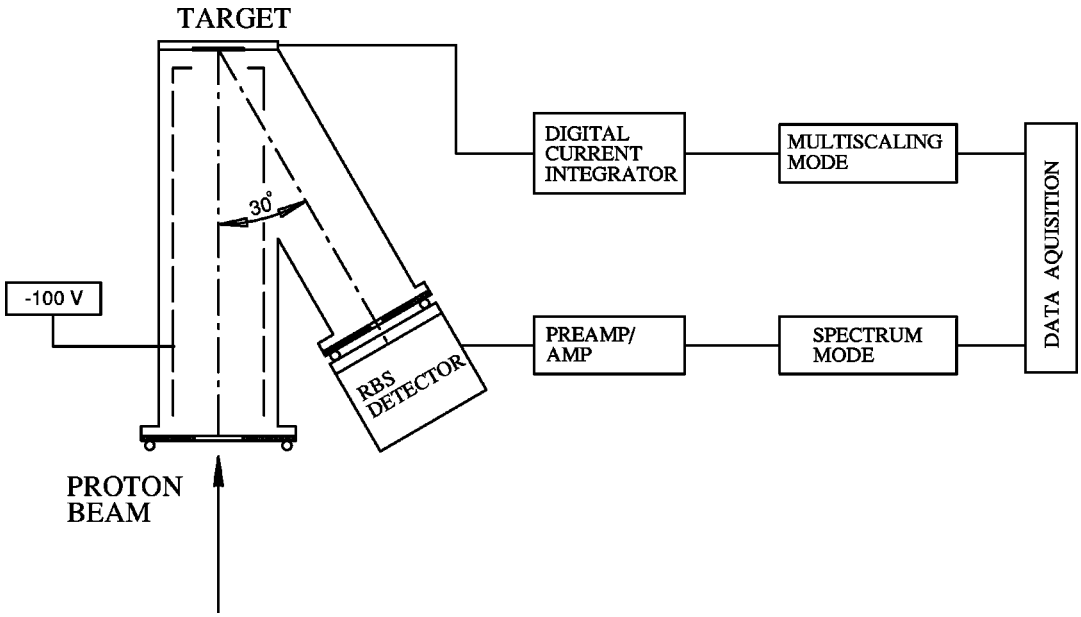

FIG. 3. Schematic setup for the activation at the accelerator. The proton beam current and the spectrum of backscattered protons were continuously monitored for later correction of the decay of activated nuclei during the irradiation and for sample degradation.

cross sections could be obtained for the ^{99}Ru$(p,\gamma)^{100}$Rh and ^{104}Ru$(p,\gamma)^{105}$Rh reactions. Another complication results from the competing (p,n) reactions. This is particularly disturbing for the (p,γ) cross section of ^{100}Ru, since the product nucleus ^{101}Rh is also produced in the ^{101}Ru(p,n) reaction.

The systematic uncertainties are summarized in Table III. Items that were not addressed in detail have been discussed in Ref. [8]. In the following paragraphs the data analysis and the results are presented for each isotope. In addition, the experimental data are compared to cross sections calculated with the Hauser-Feshbach code NON-SMOKER [11]. This code and the conclusions that can be drawn from this comparison are discussed in more detail in Sec. V.

A. ^{96}Ru$(p,\gamma)^{97}$Rh

The partial cross sections of isomer and ground state could be measured with uncertainties of less than 5%, except for the lowest energies where the 839.8 keV and 878.8 keV lines from the ground state decay were too weak for a meaningful analysis. Therefore, the ground state cross section had to be determined via the 421.5 keV line by subtracting the respective contribution from the isomer decay. Cascade-summing corrections were negligible in this case since only direct transitions to the ground state were used in the analysis.

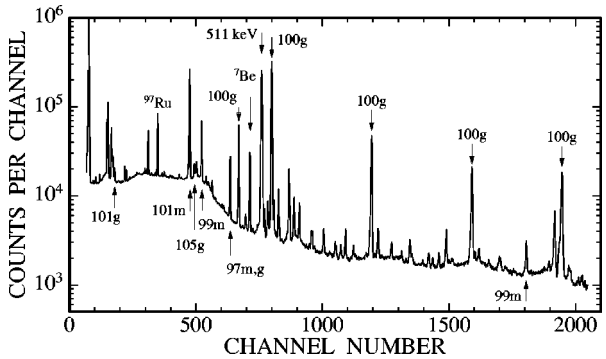

FIG. 4. Gamma-ray spectrum measured after activation of a ruthenium sample. The γ lines used in the data analysis are indicated for the various isotopes; *m* and *g* denote transitions related to the decay of isomers and ground states, respectively.

Comparison of the total (p,γ) cross section with the theoretical data in Fig. 5 shows that the statistical model overestimates the cross section by a factor of 1.8 on average. The measured cross sections and *S* factors are listed in Table IV.

B. ^{98}Ru$(p,\gamma)^{99}$Rh

The cross sections of the isomer and ground state were determined with uncertainties of 5–6 % and 8–9 %, respectively, the ground state being less accurate because of its longer half-life. For this partial cross section, cascade corrections of 14% had to be considered. At 2919 keV, the (p,n) threshold for ^{99}Ru is reached, so that additional ^{99}Rh is produced via the ^{99}Ru$(p,n)^{99}$Rh channel. Therefore, the measured cross section rises faster at higher energies than the calculated (p,γ) cross section shown in Fig. 5. When the theoretical ^{98}Ru$(p,\gamma)^{99}$Rh and ^{99}Ru$(p,n)^{99}$Rh cross sections are added, the sum is still a factor of 2 lower than the experimental data.

For proton energies between 1800 keV and the ^{99}Ru (p,n) threshold the theoretical cross section agrees well with the experimental data, while it is an order of magnitude too low for the three data points at lower energies. More experimental data at lower energies would be necessary to decide whether this represents a systematic trend or a fluctuation of the cross section around the mean value calculated with the statistical model.

C. ^{99}Ru$(p,\gamma)^{100}$Rh

For this reaction, the partial cross sections to the isomer and ground state of ^{100}Rh could not be separated, because the

TABLE II. Decay properties of the product nuclei.

Product nucleus	Reference		Half-life	Gamma-ray energy (keV)	Relative intensity per decay (%)
^{97}Rh	[19]	Ground state	30.7±0.6 min	421.55	73.7±3.8
				840.13	12.1±1.2
				878.80	9.1±0.9
		Isomer	46.2±1.6 min	421.55	12.0±1.4
				189.21	47.26±0.25
		IT[a]			4.9±0.5
^{99}Rh	[20]	Ground state	16.1±0.2 d	353.05	30.0±2.8
				528.24	33.0±3.0
		Isomer	4.7±0.1 h	340.8	70.3±4.6
				617.8	12.0±1.1
				1261.2	11.1±0.5
		IT			<0.16
^{100}Rh	[20]	Ground state	20.8±0.1 h	446.2	11.2±0.4
				539.6	78.4±2.9
				822.5	20.2±1.1
				1107.1	13.3±0.5
				1341.6	4.86±0.26
				1362.1	15.1±0.5
		Isomer	4.6±0.2 min	too short lived for detection	
		IT			~98.3
^{101}Rh	[20]	Ground state	3.3±0.3 yr	127.21	73.0±6.0
				198.0	70.8±6.0
				325.2	13.4±1.6
		Isomer	4.34±0.01 d	306.86	87.0±4.8
		IT			8.0±2.0
^{105}Rh	[20]	Ground state	35.36±0.06 h	306.1	5.1±0.3
				318.9	19.2±0.4
		Isomer	45 s	too short lived for detection	
		IT			100

[a]Isomeric transition.

4.7 min half-life of the isomer was too short compared to the adopted activation times. But since the isomer decays predominantly by internal transitions, the accumulated ground state activity could be used for deriving the total (p,γ) cross section. At high energies, all six γ transitions listed in Table II could be used for the analysis, yielding an overall uncertainty of 5%. Cascade corrections between 10% and 15% had to be considered in this case.

On average, the Hauser-Feshbach prediction and the experimental data agree within 40%, but the difference changes sign at the (p,n) threshold. Assuming complete isospin mixing (see Sec. V), the Hauser-Feshbach prediction and the experimental data agree very well below the (p,n) threshold. Above the threshold, the competition by the neutron channel is significantly overestimated by the calculation (dashed line). When explicitly considering the suppression of the (p,n) channel for pure $T^<$ states, the (p,γ) cross section is increased above the threshold and agrees well with the data (dotted line in Fig. 5), yielding an average deviation of 14%.

TABLE III. Compilation of systematic uncertainties (%).

	^{96}Ru$(p,\gamma)^{97}$Rh		^{98}Ru$(p,\gamma)^{99}$Rh			
Source of uncertainty	g.s.[a]	Isomer	g.s.	Isomer	^{99}Ru$(p,\gamma)^{100}$Rh	^{104}Ru$(p,\gamma)^{105}$Rh
Half-life	2.0	3.5	1.2	2.1	0.5	0.2
γ intensity per decay, I_γ	5.0	5.2	9.0	4.5	3.5	2.1
Isomer decay to g.s., η	0.5	0.5				
Cascade corrections			1.3	0.2	1.0	
Efficiency of γ detector, ϵ_γ				1.5		
Target thickness				3.0		
Proton beam current				1.0		

[a]Ground state.

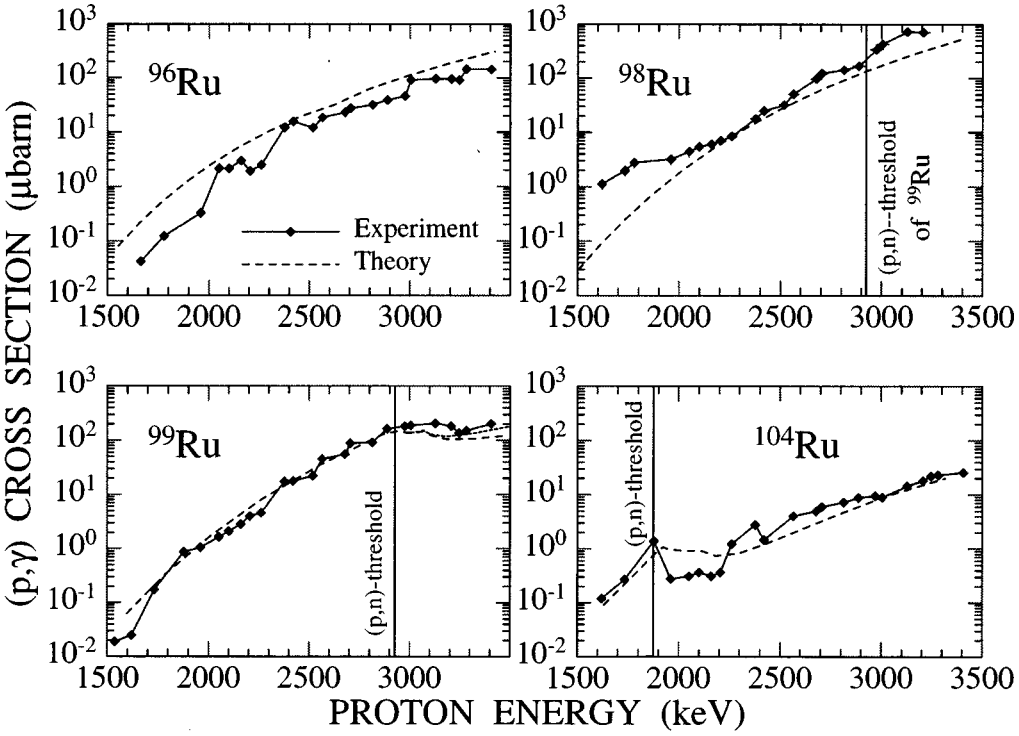

FIG. 5. The measured (p,γ) cross sections compared to statistical model calculations. The example of ^{99}Ru illustrates the isospin effect (dashed and dotted lines; see Sec. IV C).

TABLE IV. Measured (p,γ) cross sections and S factors of ^{96}Ru.

	Cross section (μb)			S factor (10^9 keV b)
Energy bin[a] (keV)	Isomer	Ground state	Total	Total
1647±14	0.014±0.001	0.028±0.002	0.042±0.003	35.9±3.1
1760±15	0.060±0.004	0.062±0.005	0.122±0.009	36.6±3.1
1940±12	0.089±0.007	0.24±0.02	0.325±0.022	22.8±1.8
2029±12	0.90±0.07	1.25±0.09	2.15±0.15	78.9±6.2
2079±12	1.19±0.09	0.94±0.07	2.13±0.15	51.2±4.0
2139±12	1.61±0.12	1.39±0.10	3.00±0.21	52.4±4.1
2182±12	0.76±0.06	1.17±0.08	1.91±0.13	25.3±1.9
2237±11	0.72±0.05	1.77±0.13	2.49±0.17	23.4±1.8
2352±11	5.99±0.42	6.07±0.39	12.1±0.7	58.4±3.9
2395±10	6.46±0.45	9.24±0.59	15.7±0.9	59.9±3.9
2494±8	7.38±0.52	4.67±0.30	12.0±0.7	27.1±1.8
2538±11	8.46±0.59	10.1±0.7	18.6±1.1	33.6±2.2
2650±7	10.8±0.8	12.4±0.8	23.2±1.4	24.4±1.6
2679±11	14.0±1.0	13.5±0.9	27.5±1.7	25.4±1.7
2787±7	17.9±1.3	14.1±0.9	31.9±1.9	18.2±1.2
2858±9	25.6±1.8	13.4±0.9	39.0±2.3	16.5±1.1
2946±6	15.9±1.1	30.4±1.9	46.3±2.8	13.7±0.9
2975±12	40.6±2.8	50.9±3.3	91.5±5.5	24.2±1.6
3095±5	36.1±2.5	60.0±3.8	96.1±5.8	16.1±1.0
3175±5	39.7±2.8	55.8±3.6	95.4±5.7	12.0±0.8
3213±6	37.7±2.7	53.3±3.4	91.1±5.5	10.0±0.6
3247±6	65.0±4.6	79.6±5.1	145±9	14.2±0.9
3372±5	61.0±4.3	82.7±5.3	144±9	9.33±0.62

[a]Values in the c.m. system.

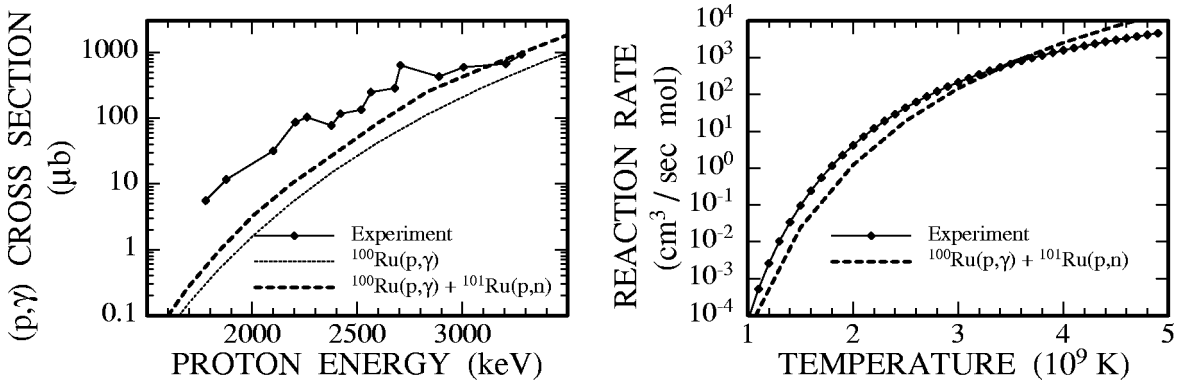

FIG. 6. The production cross section of ^{101}Rh via ^{100}Ru(p,γ) plus ^{101}Ru(p,n). Note the large discrepancies with the calculation (dashed line) at low energies.

D. ^{100}Ru$(p,\gamma)^{101}$Rh

The ^{100}Ru$(p,\gamma)^{101}$Rh reaction could not be determined in the present experiment. It is masked by the ^{101}Ru$(p,n)^{101}$Rh reaction which has a low (p,n) threshold of 1.3 MeV. Accordingly, only the sum of both reactions could be deduced corresponding to the production cross section of ^{101}Rh under proton bombardment. In this analysis the ^{100}Ru and ^{101}Ru abundances were approximated by the mean of the natural isotopic ratio, which caused an additional uncertainty of $\pm 5\%$.

At lower energies the theoretical cross section is much smaller than the experimental results (Fig. 6), but this difference vanishes around 3 MeV.

E. ^{104}Ru$(p,\gamma)^{105}$Rh

Similar to the case of ^{100}Rh, also the ^{105}Rh isomer was too short lived so that only the total cross section could be determined for this reaction (Table VI). Cascade corrections were not required for the analysis of the ground state decay. A pronounced competition cusp appears at 1871 keV where the (p,n) threshold is reached. In contrast to the corresponding feature in the ^{99}Ru cross section, the effect of this additional reaction channel is much weaker in the calculated data.

The theoretical excitation curve shown in Fig. 5 was obtained assuming complete isospin mixing. Incomplete mixing yields a slightly enhanced (p,γ) cross section above the

TABLE V. Measured (p,γ) cross sections and S factors of ^{98}Ru.

	Cross section (μb)			S factor (10^9 keV b)
Energy bin[a] (keV)	Isomer	Ground state	Total	Total
1603±6	0.19±0.02	0.93±0.10	1.12±0.11	1471±162
1714±8	0.30±0.02	1.67±0.18	1.97±0.20	895±100
1858±7	0.48±0.03	2.28±0.24	2.76±0.27	367±39
1940±12	0.59±0.04	2.62±0.28	3.21±0.32	225±24
2029±12	0.79±0.05	3.61±0.38	4.40±0.43	161±17
2078±12	0.88±0.06	4.54±0.48	5.43±0.54	141±15
2139±12	1.24±0.09	4.81±0.51	6.05±0.60	106±11
2182±12	1.22±0.08	5.77±0.61	6.99±0.69	92.6±9.8
2237±11	1.68±0.12	6.76±0.72	8.44±0.84	79.4±8.3
2352±11	5.53±0.38	12.3±1.3	17.8±1.7	85.9±9.0
2395±10	7.26±0.50	17.4±1.9	24.7±2.4	94.2±9.6
2494±8	8.18±0.57	23.7±2.5	31.9±3.1	72.1±7.3
2538±11	13.5±0.9	37.2±3.9	50.5±4.8	91.2±9.1
2650±7	21.9±1.5	74.2±7.9	96.1±9.4	101±10
2679±11	27.0±1.6	96.2±10.2	123±12	113±12
2787±7	29.6±1.8	112±12	142±14	81.1±8.1
2858±9	40.7±2.5	126±13	167±16	70.5±7.3
2946±6	45.8±2.8	293±31	339±34	100±10
2975±12	75.7±4.6	350±35	426±39	112±9
3095±5	319±19	406±40	725±59	121±9
3175±5	484±30	222±22	706±52	88.9±6.5
3213±6	825±50	270±26	1095±76	120±9
3247±6	1460±89	306±30	1766±119	173±12
3372±5	2263±138	460±45	2723±183	176±12

[a]Values in the c.m. system.

TABLE VI. Measured (p,γ) cross sections and astrophysical S factors of ^{99}Ru and ^{104}Ru

	Cross sections (μb)		S factors (10^9 keV b)	
Energy bin[a] (keV)	^{99}Ru$(p,\gamma)^{100}$Rh	^{104}Ru$(p,\gamma)^{105}$Rh	^{99}Ru$(p,\gamma)^{100}$Rh	^{104}Ru$(p,\gamma)^{105}$Rh
1463±14	0.025±0.002	0.08±0.01	150±15	481±63
1522±14	0.019±0.002	b	58.5±5.6	b
1604±6	0.025±0.002	0.12±0.01	32.8±3.1	158±15
1715±8	0.174±0.014	0.27±0.02	79.0±7.3	123±11
1858±7	0.87±0.07	1.39±0.12	116±10	185±18
1940±12	1.05±0.08	0.28±0.02	73.7±6.3	19.7±1.6
2029±12	1.64±0.13	0.31±0.03	60.2±5.2	11.4±1.2
2079±12	2.10±0.15	0.36±0.03	54.4±4.3	9.33±0.84
2139±12	2.82±0.20	0.31±0.02	49.3±3.9	5.42±0.44
2182±12	3.98±0.28	0.37±0.03	52.7±4.1	4.90±0.43
2237±11	4.58±0.32	1.24±0.09	43.1±3.3	11.7±0.94
2352±11	17.4±1.2	2.85±0.23	83.9±6.4	13.8±1.2
2395±10	17.7±1.2	1.46±0.12	67.5±5.1	5.57±0.49
2494±8	22.1±1.3	b	50.0±3.3	b
2538±11	45.1±2.7	4.02±0.28	81.4±5.5	7.26±0.55
2650±7	55.0±3.3	4.95±0.35	57.9±3.9	5.22±0.40
2679±11	88.1±5.3	6.01±0.42	81.3±5.4	5.55±0.42
2787±7	91.6±5.5	7.23±0.52	52.3±3.5	4.13±0.32
2858±9	163±8	8.85±0.53	68.9±3.9	3.74±0.25
2946±6	182±9	9.51±0.66	53.8±3.0	2.82±0.20
2975±12	188±9	8.95±0.63	49.6±2.7	2.36±0.18
3095±5	206±10	14.4±1.0	34.5±1.9	2.41±0.18
3175±5	183±9	18.1±1.3	23.0±1.3	2.28±0.17
3213±6	137±7	21.9±1.5	15.1±0.9	2.41±0.17
3247±6	151±7	23.1±1.6	14.8±0.8	2.26±0.16
3372±5	201±10	25.3±1.8	13.0±0.7	1.64±0.12

[a]Values in the c.m. system.
[b]Yield too small for meaningful analysis.

(p,n) threshold, depending on the amount of mixing chosen. This indicates that the width fluctuation corrections may underestimate the strength of the neutron channel. The combined effect of increased width fluctuation corrections and incomplete isospin mixing should be able to reproduce the experimental data at energies above 2.2 MeV and to better account for the competition cusp. A deficiency in the width fluctuation correction should also be observable below the (p,n) threshold but for a definite statement more low energy data would be needed. Nevertheless, on average there is good agreement between the theoretical cross section of Fig. 5 and the experimental results.

F. Astrophysical S factor

Since charged particle reactions are dominated by Coulomb effects, nuclear properties can be seen more clearly after converting the data into the astrophysical S factor,

$$S(E)=\frac{E\cdot\sigma(E)}{P(E)}, \tag{6}$$

with $P(E)=\exp[-31.29\ Z_1Z_2(\mu/E)^{1/2}]$ being the penetrability of the Coulomb barrier and μ the reduced mass; all energies are in the center-of-mass system. The resulting values of the S factors are listed in Tables IV–VI together with the cross sections, except for the special case of ^{100}Ru (Table VII). The comparison of an experimental and a theoretical S factor is shown in Fig. 7 for the example of ^{96}Ru. Obviously, the structures in the measured cross section appear much more clearly in the S factor.

G. Reaction rates

The reaction rates for proton captures in the ground state of the target nucleus were calculated from the measured cross sections by folding the differential data with the Maxwell-Boltzmann distribution of the particle velocities:

$$\langle\sigma v\rangle=\left(\frac{8}{\pi\mu}\right)^{1/2}\frac{N_A}{(kT)^{3/2}}\int_0^\infty\sigma(E)E\ \exp\left(-\frac{E}{kT}\right)dE, \tag{7}$$

where N_A is Avogadro's number and kT the thermal energy. Since the proton energy range covered by the experiment is only sufficient to calculate rates in the temperature range between roughly 2 and 3 GK, the experimental cross sections have been extended to lower and higher proton energies by

TABLE VII. The production of ^{101}Rh under proton bombardment: the sum of the ^{100}Ru$(p,\gamma)^{101}$Rh and ^{101}Ru(p,n) ^{101}Rh reactions.

Energy bin[a] (keV)	^{101}Rh production cross section (μb) Isomer	Ground state	Total
1463±14	0.010±0.001	b	b
1604±6	0.095±0.008	b	b
1760±15	0.159±0.014	5.42±1.08	5.58±1.08
1858±7	0.201±0.016	11.4±2.3	11.6±2.3
1940±12	0.207±0.016	b	b
2029±12	0.567±0.045	b	b
2079±12	1.60±0.13	30.0±4.5	31.6±4.6
2139±12	2.84±0.23	b	b
2182±12	2.84±0.23	83.5±12.5	86.3±12.7
2237±11	5.43±0.43	97.5±14.6	103±15
2352±11	12.7±1.0	64.0±9.6	76.7±10.6
2395±10	17.5±1.2	99.1±14.9	117±16
2494±8	25.4±1.8	108±16	133±18
2538±11	53.2±3.7	194±19	247±23
2650±7	69.8±4.9	216±22	286±27
2679±11	110±8	524±47	634±53
2787±7	118±8	b	b
2858±9	202±14	223±20	425±34
2975±12	293±18	299±27	592±45
3095±5	356±21	b	b
3175±5	353±21	325±29	678±50
3213±6	357±21	b	b
3247±6	572±29	351±28	933±57
3372±5	803±40	b	b

[a]Values in the c.m. system.
[b]Yield too small for meaningful analysis.

means of the calculated cross sections after normalization to the measured data in the region of overlap. For stellar reaction rates also proton captures on thermally populated excited states have to be taken into account. This was done by multiplying the ground state reaction rates for each isotope with a temperature-dependent correction factor that was determined by comparing theoretical stellar and ground state reaction rates. Figure 8 shows that this correction can be large for temperatures above 2 GK (for example, 30% for ^{99}Ru and ^{104}Ru at 3 GK).

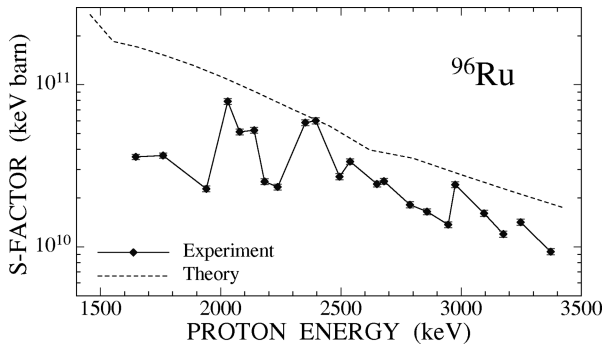

FIG. 7. The astrophysical S factor for the ^{96}Mo(p,γ) reaction exhibits significant structures due to the low level density near magic neutron number $N=50$, in contrast to the calculation (dashed line).

The resulting new stellar reaction rates are presented in Table VIII and are compared to the purely theoretical rates in Fig. 9. It can be seen that differences in the shape of the experimental and calculated cross sections are washed out in the rates, particularly at low temperatures.

For the easier use of these data in complex p-process networks, the curves in Fig. 9 have been fitted according to Woosley *et al.* [12]:

$$\langle \sigma v \rangle = T_9^{-2/3} \exp[A-(\tau/T_9^{1/3})(1+BT_9+CT_9^2 + DT_9^3)] \ \text{cm}^3/(\text{s mol}), \quad (8)$$

where $\tau=4.2487\,(Z_1^2Z_2^2\mu)^{1/3}$. A similar parametrization has been suggested by the NACRE Collaboration [13], starting from a modified rate

$$N\langle \sigma v \rangle_{\text{mod}} = N\langle \sigma v \rangle T_9^{-2/3} \exp[4.2486(Z_1Z_2\mu/T_9)^{-1/3}] = \exp(A+BT_9+CT_9^2). \quad (9)$$

The respective parameters are summarized in Table IX. These fits represent reasonably good approximations of the experimental rates, the four-parameter approach of Ref. [12] showing slightly smaller deviations. In general, the quality of the fits corresponds to the experimental uncertainties, at least at the relevant p-process temperatures.

V. STATISTICAL MODEL CALCULATIONS

The experimental (p,γ) data can be compared with the theoretical cross sections used in p- and rp-process nucleosynthesis studies, which are typically calculated within the framework of the statistical Hauser-Feshbach model. In this work, cross sections and reaction rates were calculated with the semiempirical and globally parametrized code NON-SMOKER [11], which is an improved version of the well-known statistical model code SMOKER [14]. The basic ingredients for the calculation of (p,γ) reaction rates are the transmission coefficients for protons and γ rays describing the transitions from the compound nucleus into the ground and excited states of the target and final nucleus, respectively. The proton transmission coefficients were calculated by solving the Schrödinger equation for the microscopic (purely theoretical) optical potential of Jeukenne *et al.* [15].

The γ transmission coefficients were limited to $M1$ and $E1$ transitions. The smaller and less important $M1$ transitions were treated in a simple single-particle approach, while for $E1$ transitions a semiempirical parametrization of the shape and position of the giant dipole resonance (GDR) was used.

Width fluctuation corrections were applied to all particle and radiative transmission coefficients (see Ref. [16] and references therein). These corrections account for correlations between the entrance and exit channels leading to deviations from a purely statistical description. The most prominent effect of width fluctuation corrections is an enhancement of elastic scattering, since in this case the entrance and exit channels are identical. This requires a renormalization of all transmission coefficients, which results in a redistribution of the strength from the dominant channel into elastic and weak channels. The transmission coefficients have to be calculated

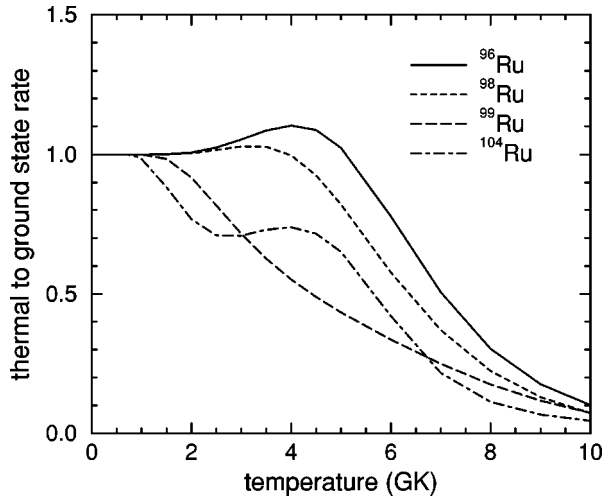

FIG. 8. The ratio of the proton capture reaction rate for a thermally excited target nucleus in a stellar plasma to a target nucleus in the ground state as a function of temperature.

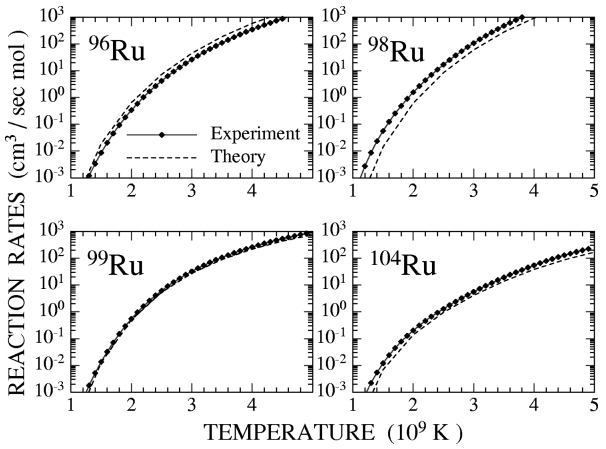

FIG. 9. The stellar rates for the (p,γ) reactions on ^{96}Ru, ^{98}Ru, ^{99}Ru, and ^{104}Ru. In the temperature range of the p process between $2<T_9<3$ there is relatively good agreement with the calculations (dashed lines).

for all excited states in the target or final nucleus that can be populated. The maximum excitation energy for these states is determined by the channel separation energy (and thus by the nuclear ground state masses) and the temperature.

In the investigated energy range of the stable Ru isotopes this maximum excitation energy is 3.4 MeV in the proton channel and 7–9 MeV in the γ channel, well above the energy region where all excited states are known experimentally. Therefore, the theoretical level density, which is calculated in the backshifted Fermi-gas model, becomes crucial. Recently, the calculation of level densities has been improved by considering an energy-dependent level density parameter and by inclusion of microscopic information [16]. The pairing gap (which determines the backshift) and the microscopic corrections that account for deviations from the average level density were both taken from the 1992 finite range droplet model [17].

TABLE VIII. Total (p,γ) rates for ^{96}Ru, ^{98}Ru, ^{99}Ru, and ^{104}Ru (cm^3/s mol).

Temperature (10^9 deg)	^{96}Ru	^{98}Ru	^{99}Ru	^{104}Ru
1.5	0.009	0.057	0.014	0.012
1.6	0.020	0.124	0.032	0.024
1.7	0.045	0.254	0.072	0.044
1.8	0.093	0.487	0.149	0.077
1.9	0.181	0.891	0.293	0.127
2.0	0.336	1.56	0.545	0.200
2.1	0.598	2.65	0.958	0.307
2.2	1.02	4.36	1.61	0.457
2.3	1.68	6.98	2.61	0.660
2.4	2.67	10.9	4.07	0.930
2.5	4.13	16.7	6.14	1.28
2.6	6.23	25.1	8.99	1.77
2.7	9.19	36.9	12.8	2.40
2.8	13.3	53.5	17.8	3.22
2.9	18.8	76.2	24.2	4.25
3.0	26.1	107	32.3	5.56
3.1	35.8	148	42.3	7.24
3.2	48.3	201	54.5	9.35
3.3	64.2	270	69.1	12.0
3.4	84.4	359	86.4	15.2
3.5	110	472	107	19.2
3.6	140	609	130	23.9
3.7	178	779	158	29.7
3.8	224	988	189	36.6
3.9	279	1240	223	44.8
4.0	345	1544	262	54.5

Since the application of the statistical model is justified for all temperatures and reactions discussed in this work (see Fig. 9 of Rauscher *et al.* [16]), the comparison of the present experimental and theoretical data should reveal the quality of the global parametrization of the nuclear properties discussed in the previous paragraph.

The deviations between the theoretical and experimental cross sections for the (p,γ) reactions on ^{96}Ru, ^{98}Ru, ^{99}Ru, and ^{100}Ru (in their ground state) measured in this work have been described in Sec. IV. Together with the recently reported (p,γ) cross sections for ^{92}Mo, ^{94}Mo, ^{95}Mo, and ^{98}Mo [8] this set of experimental data allows a first critical comparison for the statistical model calculations of (p,γ) cross sections and reaction rates in the $A=92-100$ range.

It has to be noted that the experimental (p,γ) cross sections for Mo isotopes were found to exceed the statistical model calculations systematically by factors of 2–4 in Ref. [8]. This was due to an erroneous treatment of charged spin-1/2 projectiles in the version of the code SMOKER used in that work, which led to a systematic underestimation of proton-induced cross sections by exactly a factor of 2. Accordingly, the true differences between the experimental data and the calculated values are smaller by that factor, and are included in Table X.

TABLE IX. Fit parameters for the temperature dependence of the investigated (p,γ) rates.

Reaction	A	B	C	D
Parametrization according to Woosley *et al.* [12]				
^{96}Ru$(p,\gamma)^{97}$Rh	44.19	3.98×10^{-2}	-3.73×10^{-3}	3.64×10^{-4}
^{98}Ru$(p,\gamma)^{99}$Rh	47.93	7.83×10^{-2}	-1.10×10^{-2}	8.37×10^{-4}
^{99}Ru$(p,\gamma)^{100}$Rh	42.55	-9.55×10^{-3}	1.05×10^{-2}	-7.59×10^{-4}
^{104}Ru$(p,\gamma)^{105}$Rh	48.59	0.106	-6.70×10^{-3}	-7.67×10^{-5}
Parametrization according to the NACRE Collaboration [13]				
^{96}Ru$(p,\gamma)^{97}$Rh	43.10	-0.958	5.01×10^{-2}	
^{98}Ru$(p,\gamma)^{99}$Rh	45.64	-1.614	0.145	
^{99}Ru$(p,\gamma)^{100}$Rh	43.34	-0.673	-4.80×10^{-2}	
^{104}Ru$(p,\gamma)^{105}$Rh	46.20	-3.293	0.321	

The observed differences between experiment and calculation range between 12% and a factor of 2. The average deviation of about 60% corresponds well to the expected accuracy of the statistical model approach with a global parametrization [16]. The largest deviations occur for ^{96}Ru, ^{98}Ru, ^{95}Mo, and ^{98}Mo. In the case of ^{98}Mo, however, the differences are entirely due to an overestimation of the cross section just above the (p,n) threshold, which is a very sensitive energy range as discussed below. Table X yields no evidence for a systematic trend of these discrepancies with proton or neutron number.

Obviously, large deviations between experimental and theoretical cross sections occur right above the (p,n) threshold, e.g., in the ^{95}Mo, ^{98}Mo, ^{99}Ru, and ^{104}Ru data, where the cross sections show a pronounced decrease as a consequence of the competing neutron channel. The calculation of these competition cusps for proton capture reactions has been shown [18] to be sensitive to the treatment of isospin mixing and width fluctuation corrections.

The code NON-SMOKER allows one to study isospin effects [11] due to incomplete isospin mixing in the nuclear states. Standard Hauser-Feshbach calculations usually neglect isospin which is equivalent to assuming completely isospin-mixed states. Incomplete isospin mixing leads to a suppression of the neutron channel in proton-induced reactions and thus to an enhancement of the (p,γ) cross section above the (p,n) threshold, compared to calculations with complete isospin mixing. Incomplete isospin mixing may appear when the first isobaric analog state in the compound nucleus is above or closely below the neutron threshold of the compound nucleus. This is the case for the (p,γ) reactions on ^{99}Ru and ^{104}Ru.

As has been discussed before (Sec. IV C), the theoretical ^{99}Ru$(p,\gamma)^{100}$Rh cross section is improved when including isospin effects. The same should be true for ^{104}Ru, but in that case the theoretical cross section is already too large in the critical energy range and it will be further enhanced by the isospin effect (Sec. IV E). This seems to indicate that the applied width fluctuation corrections are underestimating the enhancement of the neutron channel for ^{104}Ru. A similar underestimation can be seen in the case of ^{98}Mo. However, the treatment appears to be correct for ^{99}Ru and ^{95}Mo. This could be attributed to a deformation dependence of the width fluctuation correction, although this claim still awaits a theoretical justification.

In view of this situation it appears premature to attribute the problems in describing the competition cusps to a deficiency in the treatment of width fluctuation corrections. More data are needed which cover a large energy interval above and below the (p,n) threshold, as the application of width fluctuation corrections also has an impact on the cross sections below the threshold. Thus, it can be disentangled from isospin effects which only influence cross sections above the threshold. Nevertheless, even comparably large uncertainties in the prediction of competition cusps have only a small effect on the astrophysical reaction rates, since the cross section is averaged over the Gamow window with a typical width of 1–3 MeV for the cases discussed here.

VI. SUMMARY

The proton capture cross sections of the stable ruthenium isotopes 96, 98, 99, and 104 have been measured by means of the activation method in the proton energy range between 1.5 and 3 MeV. In total, six (p,γ) cross sections for populating ground states and isomers in four different Rh isotopes could be determined simultaneously with systematic uncertainties of typically 4–5 %. Together with a similar set of data for a series of Mo isotopes, these results represent the basis for a first comprehensive judgment of the accuracy obtained by the Hauser-Feshbach approach for nuclei in a relevant mass range for the nucleosynthesis of light p nuclei. It is found that for theoretical reaction rates calculated with the NON-SMOKER code an accuracy of about 60% can be expected, at least for target nuclei near stability. The lack of systematic deviations indicates that the accuracy is limited rather by the global character of the method than by significant deficiencies in the adopted model parameters.

TABLE X. Average ratio of experimental and theoretical reaction cross sections. The experimental Mo data are from Ref. [8].

^{96}Ru	^{98}Ru	^{99}Ru	^{104}Ru	^{92}Mo	^{94}Mo	^{95}Mo	^{98}Mo
0.55	2.11	1.14	1.38	0.88	1.55	2.20	0.46

ACKNOWLEDGMENTS

We would like to thank G. Rupp for his invaluable skill in solving all technical problems as well as E.-P. Knaetsch, D. Roller, and W. Seith for providing excellent proton beams during the activations. We are also very much indebted to R. Fromknecht for the RBS measurements, to D. Hentschel and S. Fetzner for the XRF analyses, and to V. Kleber for her assistance in data analysis. One of us (T.R.) is supported by the Austrian Academy of Sciences.

[1] E. Burbidge, G. Burbidge, W. Fowler, and F. Hoyle, Rev. Mod. Phys. **29**, 547 (1957).
[2] M. Rayet, *et al.* Astron. Astrophys. **298**, 517 (1995).
[3] W. Howard, B. Meyer, and S. Woosley, Astrophys. J. **373**, L5 (1991).
[4] H. Schatz, *et al.* Phys. Rep. **294**, 167 (1998).
[5] R. Cannon, in *Nuclei in the Cosmos*, edited by F. Käppeler and K. Wisshak (IOP, Bristol, 1993), p. 619.
[6] C. L. Fryer, W. Benz, and M. Herant, Astrophys. J. **460**, 801 (1996).
[7] R. Chevalier, Astrophys. J. **459**, 322 (1996).
[8] T. Sauter and F. Käppeler, Phys. Rev. C **55**, 3127 (1997).
[9] W. Chu, J. Mayer, and M. Nicolet, *Backscattering Spectrometry* (Academic Press, New York, 1978).
[10] J. Ziegler, *Handbook of Stopping Cross-Sections for Energetic Ions in all Elements* (Pergamon Press, New York, 1980), Vol. 5.
[11] T. Rauscher and F.-K. Thielemann, in *Atomic and Nuclear Astrophysics*, edited by A. Mezzacappa (IOP, Bristol, in press).
[12] S. Woosley, W. Fowler, J. Holmes, and B. Zimmerman, At. Data Nucl. Data Tables **22**, 371 (1978).
[13] C. Angulo, P. Descouvemont, and M. Arnould, in *Nuclear Data for Science and Technology*, edited by A. Ventura, G. Reffo, and C. Grandi (Italian Physical Society, Bologna, 1997), p. 1543.
[14] F.-K. Thielemann, M. Arnould, and J. Truran, in *Advances in Nuclear Astrophysics*, edited by E. Vangioni-Flam *et al.* (Editions Frontières, Paris, 1986), p. 525.
[15] J. P. Jeukenne, A. Lejeune, and C. Mahaux, Phys. Rev. C **16**, 80 (1977).
[16] T. Rauscher, F.-K. Thielemann, and K.-L. Kratz, Phys. Rev. C **56**, 1613 (1997).
[17] P. Möller, J. R. Nix, W. D. Myers, and W. J. Swiatecki, At. Data Nucl. Data Tables **59**, 185 (1995).
[18] J. L. Zyskind *et al.*, Nucl. Phys. **A343**, 295 (1980).
[19] B. Haesner and P. Luksch, Nucl. Data Sheets **46**, 607 (1985).
[20] R. Firestone, in *Table of Isotopes*, edited by V. Shirley (Wiley, New York, 1996).